Hindawi
Advances in Civil Engineering
Volume 2021, Article ID 9750447, 15 pages
https://doi.org/10.1155/2021/9750447

Research Article

Water Inrush Risk Assessment Based on AHP and Advance Forecast Approach: A Case Study in the Micangshan Tunnel

Tao Song[1,2], **Jun Zeng**[1,2], **Jiaji Ma**[1,2], **Chunchi Ma**[1,2], **Tianbin Li**[1,2] and **Tao Xia**[3]

[1]*College of Environment and Civil Engineering, Chengdu University of Technology, Chengdu 610059, Sichuan, China*
[2]*State Key Laboratory of Geohazard Prevention and Geoenvironment Protection, Chengdu University of Technology, Chengdu 610059, Sichuan, China*
[3]*The Civil Engineering Group Corporation of China Construction Second Engineering Bureau Ltd., Beijing, China*

Correspondence should be addressed to Chunchi Ma; machunchi17@cdut.edu.cn

Received 8 May 2021; Revised 28 September 2021; Accepted 5 October 2021; Published 28 October 2021

Academic Editor: Angelo Aloisio

Water inrush is a serious geological disaster in tunnel. For the effective prevention and control of the occurrence of water inrush, a static-dynamic water inrush risk assessment method is proposed by considering the Micangshan tunnel as an example. First, four possible types of water inrush phenomenon are identified based on the geological and hydrogeological conditions of the tunnel: water inrush in water-bearing cracks, fault fracture zones, karst pipelines, and karst caves. Next, evaluation indexes that affect water inrush are determined. By combining the index weight value calculated by analytic hierarchy process (AHP) with the index quantitative value, the static water inrush disaster evaluation model is established, which provides a basis for tunnel design. Finally, with the combination of the static evaluation model and advanced forecast method, a dynamic risk prediction method of water inrush is established, which provides guidance for safe construction. The results confirm that the proposed method is a reliable theoretical basis for early assessment and prediction of tunnel water inrush disasters.

1. Introduction

Detection of anomalous geological structures such as fault zones, faults, aquifers, and karsts in the process of tunnel construction is challenging owing to their large buried depth and length of the tunnel [1–4]. In particular, during the construction of a tunnel in a complex karst area, high water pressure makes the surrounding rock unstable, resulting in a water gushing disaster, which in turn may cause delay in the construction, economic loss, and even serious casualties [5, 6]. Therefore, the prediction of the water gushing phenomenon in a tunnel is a key step in tunnel construction [7].

The analytic hierarchy process (AHP) by considering the several evaluation indexes of water inrush has been widely used as a decision support tool to solve complex decision-making problems [8]. Lyu et al. [9–12] applied remote sensing and GIS coupled with AHP techniques for delineating potential groundwater zones in semiarid areas. A hierarchical structure of multilevel goals, standards, substandards, and alternatives has been established [13]. Wang et al. [14] used a fuzzy AHP to construct water inrush indices of coal seam floors based on geological, hydrogeological, floor aquitard, and mine-size factors for predicting water inrush through coal seam floors. Xue et al. [15] selected seven main factors, namely, the surrounding rock grade, rock integrity, overburden thickness, seawater thickness, tunnel section, permeability coefficient, and construction technology level, as risk assessment indicators for the evaluation model. Zhang et al. [16] considered the karst geological conditions and selected nine main factors such as ground water level, land form and physiology, attitude of rock formation, and unfavorable geological conditions as the evaluation indexes affecting water inrush in tunnels. However, the existing prediction models do not introduce factors affecting the types

of water inrush. First, rock roofs with different thickness have distinct failure patterns under complex pressure [17, 18]. Moreover, the uncertainty of the geological conditions in front of the tunnel face causes different hydrogeological conditions and types of water inrush phenomenon in different areas. Second, in the AHP, the consistency test of the judgment matrix is complicated and requires multiple adjustments, and most of the existing evaluation models lack quantitative indicators of evaluation factors to analyze the risk of water inrush and hazards [19]. Therefore, it is necessary to introduce evaluation indexes of the water inrush disaster types into the prediction model in order to establish a quantitative and qualitative water inrush prediction method.

Water inrush and mud inrush and their early warning system focusing on risk assessment and advanced prediction have been extensively researched. At present, advanced prediction methods of tunnels, such as tunnel seismic prediction (TSP), tunnel reflection tomography (TRT), ground penetrating radar (GPR) detection, infrared water detection, and advanced borehole detection, can determine different response characteristics with respect to the groundwater according to the specific characteristics of each detection method, and a follow-up dynamic prediction method is adopted to predict the location of water inrush disaster in the tunnel. For example, to prevent unforeseen unfavorable geological conditions, it is necessary to investigate the geological and hydrogeological conditions in front of tunnel excavation faces in the construction stage [20]. According to the properties of seismic waves, TSP is used as a long distance prediction method, and for this method, explosives are used as the seismic source to identify anomalies related to geological structures and aquifers [21–23]. Yamatoto et al. [24] developed a three-dimensional reflector tracking system, namely, TRT, which can detect the geological conditions at 100–150 m in front of the tunnel face. For the improvement of detection and interpretation, ground penetrating radar is used as a short-term prediction method [25, 26]. With the interpretation of GPR images, abundant useful information can be extracted for describing and distinguishing groundwater and its specific location [27]. Corbeanu et al. [28] used GPR attributes to predict 3D fluid permeability and mudstone distribution in east-central Utah. GPR attributes have also been studied in the geological exploration of karst tunnels [27]. Advance drilling can detect the softness and hardness of formation rock, the integrity of rock mass, and the distribution location of possible faults and water inrush, through the analysis of the propulsion rate, rotation speed, and exposed lithology [29]. However, because the relationship between the interpretation standard of advanced prediction methods and geological structure is nonlinear, widespread uncertainty and multiple results exist in the interpretation of geological advanced prediction [30, 31]. Therefore, it is necessary to deeply understand the response characteristics of various advanced prediction methods for groundwater, establish a dynamic risk assessment system, and predict the risk of water inrush disaster in the construction process.

In this study, we established a static-dynamic risk assessment method to predict water inrush hazards taking the Micangshan tunnel as the research object. First, the types of water inrush disasters were classified based on engineering geological and hydrogeological conditions. According to the analytic hierarchy process and the scoring method, a quantitative and qualitative static evaluation method was established to quantify the risk of water inrush hazard, thereby providing a basis for the design stage. Second, according to the static evaluation method, three dynamic prediction methods corresponding to the water inrush disaster in the construction process were established. Finally, the reliability and applicability of the method were verified with an example for the tunnel water inrush disaster prediction, prevention, and control to provide reference.

2. Engineering Profile

2.1. Site and Geology. The Micangshan tunnel connects the Shanxi Province with the Sichuan Province as shown in Figure 1. It is a separated deep-buried super-long twin tunnel and is a major engineering structure in the Taoba Expressway. Its beginning-ending mileage is K39 + 733–K53 + 527; it is 13.8 km long and has the maximum buried depth of approximately 1055 m. The tunnel entrance is located in the Nanzheng County of Hanzhong City, Shaanxi Province. The distribution of precipitation in this area is uneven, mainly concentrated from July to September, accounting for 53% of the whole year, with an average annual precipitation of 920 mm. The exit of the tunnel is located in the Nanjiang County of Bazhong City, Sichuan Province. This area has abundant precipitation, with an average precipitation of 1828 mm for many years. The surface water body in the geological area of the tunnel is well developed, with most of the gullies developing into tree shape and most of the smaller gullies having only seasonal water. The groundwater in the tunnel area is mainly divided into clastic rock fissure water, karst fissure water, and bedrock fissure water.

2.2. Geological Structure. The geological structure of the Micangshan tunnel is shown in Figure 2. Based on the borehole Z1–Z4 data, the lithology mainly comprises argillaceous siltstone, argillaceous limestone, dolomite, and quartz diorite. This well-developed structure consists of two syncline structures, i.e., Xiaoba and Neutron Mountain, and one anticline structure, i.e., Daba, as well as six fault fracture zones (F1–F6). Based on the borehole Z1 data, the axial strata of the Xiaoba syncline structures are severely crumpled, having the characteristics of karst. According to the exposure of borehole Z4, the Daba anticline structure is located in the concave valley, and the rock masses at its two wings and core are magmatic rocks with massive structure. The limestone section belongs to the regional karst section, with weak to medium karst development, relatively well-developed fissures, abundant water content, and high water head that bears high pressure. There are surface karst caves, shafts, and funnels in some sections.

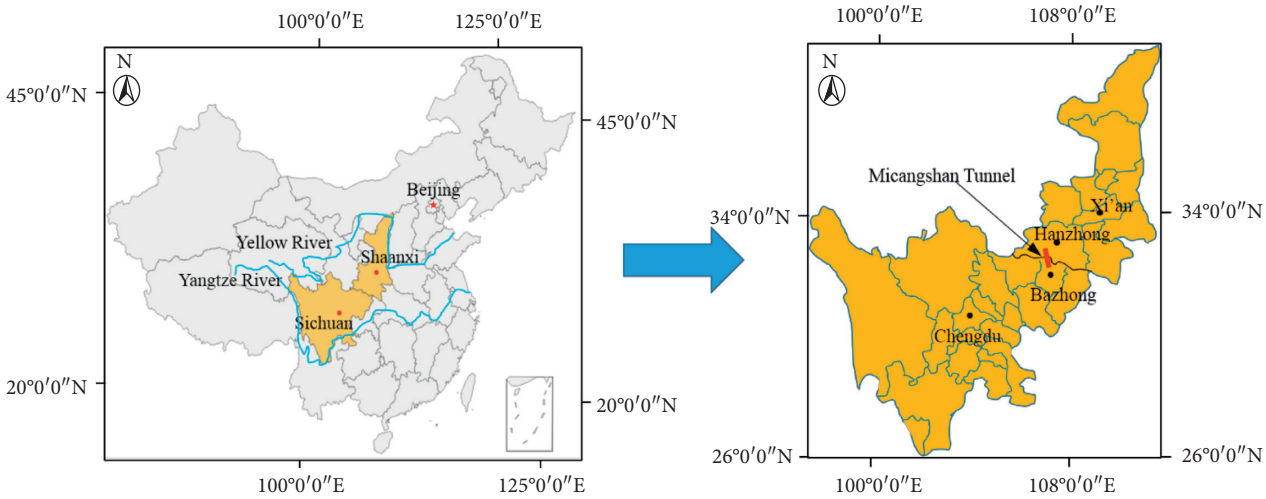

Figure 1: Location of the Micangshan tunnel.

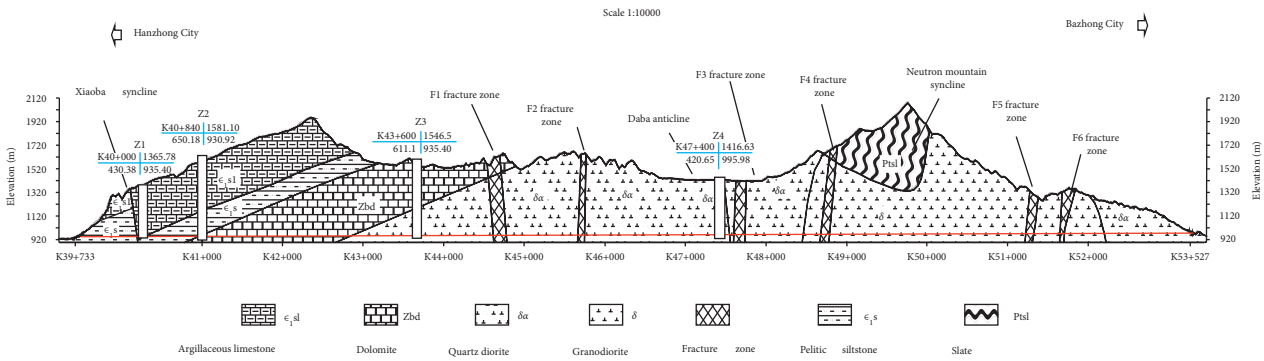

Figure 2: Overview of the geological structure of the Micangshan tunnel.

There is a joint dense zone in the position of the rock contact zone, syncline structure, and fault fracture zone. Tectonics and waterproofing effect make the soluble rocks in the region beneficial to the recharging of groundwater and the dissolution of soluble rock components, resulting in a strong degree of karst development and various dissolution forms in this area.

2.3. Prediction of Types of Water Inrush. The water inrush of the tunnel involves three aspects: the disaster source, water inrush channel, and antioutburst structure. The disaster source is the most important source of power and material basis for the water inrush. The possibility and states of water inrush in the Micangshan tunnel are predicted according to its underlying geological and hydrogeological conditions. Four main types of water inrush are identified: water inrush in water-bearing cracks, fault fracture zones, karst pipelines, and karst caves [32, 33].

2.3.1. Water Inrush in Water-Bearing Cracks. As shown in Figure 3, when excavating in rock strata with poor permeability, the stress around the surrounding rock constantly changes because the disturbance caused by tunnel excavation destroys the original seepage balance system. Under the combined action of high groundwater pressure head and surrounding rock stress, the groundwater weakens the fractured rock mass and forms water wedges in it. When the groundwater pressure in the fracture plane exceeds the ultimate strength of the fracture expansion in the rock mass, the water-bearing fracture may expand and split gradually [32, 33]. The scouring and enlarging effect of groundwater will expand the water inrush channel continuously, which leads to the groundwater directly gushing into the tunnel or infiltrating into the tunnel from the cracks, forming a water gushing channel and causing the water inrush phenomenon.

2.3.2. Water Inrush in Fault Fracture Zones. As shown in Figure 4, the special tectonic action of the fault leads to the formation of a large number of fracture zones in the rock mass, and most of the fillers in the fault zone are angular and of different sizes. Because the water permeability of the fault fracture zone is higher than that of the aquifer rock mass, strong tangential stress and circumferential stress may appear in the fault fracture zone, leading to the relaxation of the original fault zone, further expansion of the original fracture, and even formation of new cracks. At the same time, groundwater can collect between two rock masses in the

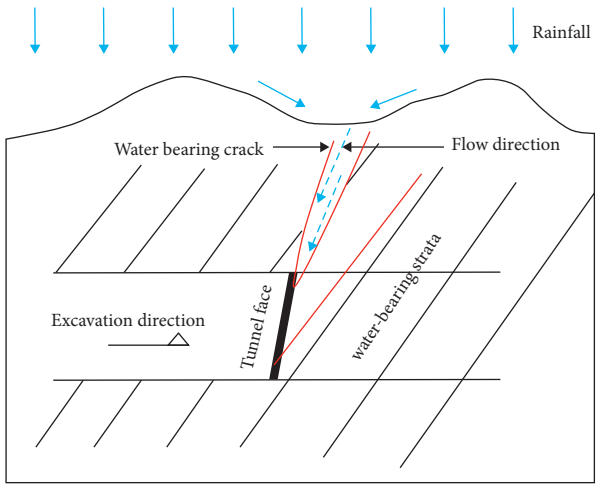

Figure 3: Diagram of water inrush in a water-bearing crack.

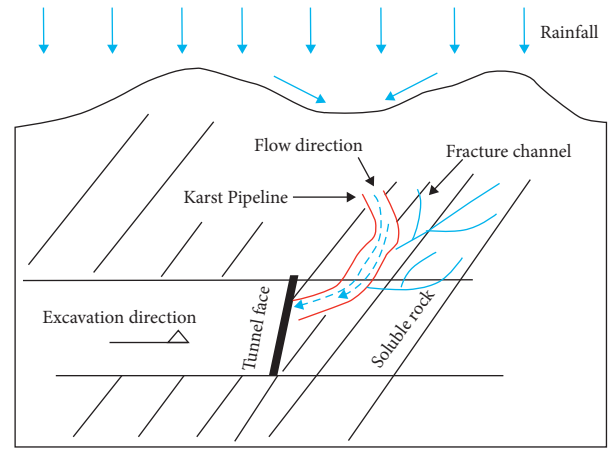

Figure 5: Diagram of water inrush in a karst pipeline.

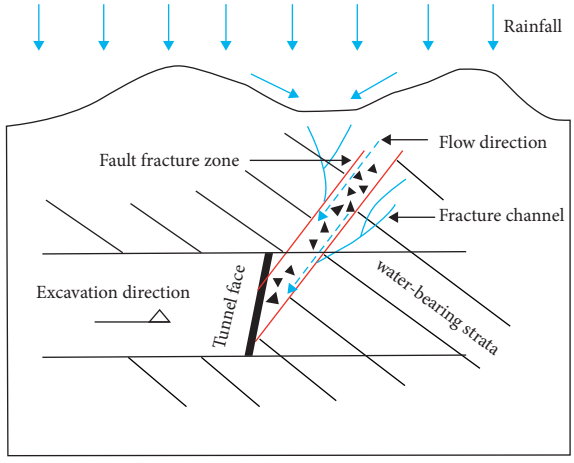

Figure 4: Diagram of water inrush in a fault fracture zone.

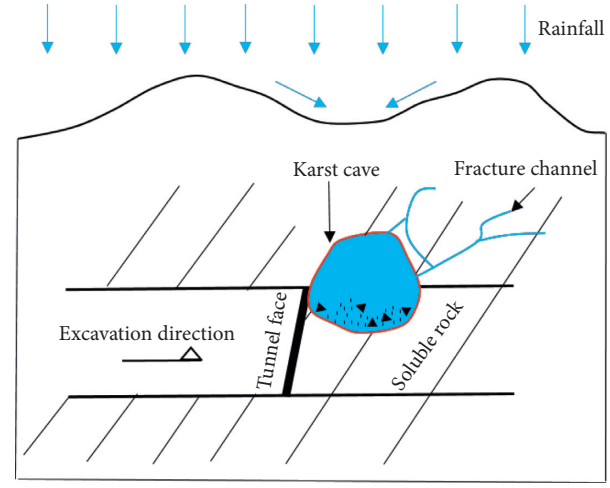

Figure 6: Diagram of water inrush in a karst cave.

faults, providing space and channels for the storage and migration of groundwater. When tunnel excavation is performed at such faults, the amount of water gushing may be considerably large [32, 33].

2.3.3. Water Inrush in Karst Pipelines. As shown in Figure 5, the topographical and lithological effects cause low-lying areas to easily form basins and become recharge areas of karst groundwater. Owing to the long-term action of surface water or groundwater, the rock is eroded, and the presence of water-bearing pipes with good connectivity, strongly permeable water-bearing strata, fissures, or other water-bearing structures with good permeability in the surrounding rock results in the formation of karst pipelines [32, 33]. The excavation of the tunnel in the areas with karst pipelines directly reveals the water-bearing structure in the surrounding rock, which leads to the water inrush phenomenon in the tunnel.

2.3.4. Water Inrush in Karst Caves. As shown in Figure 6, due to geological tectonics, the fissures and interlayer sliding spaces formed in the soluble rock strata create the original space for the formation and expansion of karst caves. Under the action of chemical dissolution for a long time, the groundwater carries sediment, debris, and other materials into the karst cave through the fracture channel, forming a filling medium in the karst cave, together with the source rock, gravel, breccia, and other materials. During the construction of the tunnel, the karst caves are disturbed and they directly push over the waterproof layer; when they reach the critical state, because of the strong water pressure, the previously deposited materials are flushed out, forming a geological hazard of water and mud inrush into the tunnel [32, 33].

3. Scoring Method and Analysis of Static Water Inrush Disasters

A static water inrush disaster assessment model is a risk assessment system of the water inrush phenomenon based on the AHP and the scoring method. First, the evaluation indexes affecting the water inrush risk are determined. Based on the AHP, each evaluation index is further

divided into several evaluation factors, and the weight of each index is determined. Second, the disaster risk value is associated with the quantitative score of each evaluation index by a certain method, and the quantitative value that can accurately reflect the characteristics of environmental factors is input. According to the scoring method, the effect of the quantitative standard of each basic evaluation index or evaluation factor on the development of things is scored. Finally, a numerical model is established using the reverse-order superposition method, and the actual analysis is combined with it to determine the final judgment.

3.1. AHP Analysis Method. The AHP, which was recommended by Saaty [34], is a hierarchical weighting multiobjective comprehensive evaluation decision analysis method based on the network system theory. This combined quantitative-qualitative analysis is used for multiobjective decision-making and evaluation for complex problems. It involves the following major steps.

Step 1. Establish AHP structure model.

In this step, the overall goal is established, the decision-making problem is decomposed in detail, hierarchical and organized characteristics are formed, and a multilevel gradient structure model is developed. In the developed model, the elements are divided into the top, middle, and lower layers according to their attributes and interrelationships. The elements of the upper layer are composed of the elements of the lower layer, and they play a dominant role in determining the relevant elements of the subsequent layer. A linear series connection is adopted to build a hierarchical level of characteristics.

Step 2. Establish the comparative judgment matrix.

In this step, a certain factor U is considered the standard of the judgment matrix, based on which the factors of the lower layer are compared, and the n-order judgment matrix is obtained as shown in the following equation:

$$U = \begin{bmatrix} a_{11} & a_{12} & \cdots & a_{1n} \\ a_{21} & a_{22} & \cdots & a_{2n} \\ \cdots & \cdots & \cdots & \cdots \\ a_{n1} & a_{n2} & \cdots & a_{nn} \end{bmatrix}, \quad (1)$$

where $a_{ij} = 1/a_{ji}\,(i \neq j)$, $a_{ij} = 1\,(i = j)$.

Suppose there are n factors (U_1, U_2, ..., U_n) in the same layer; then all the factors are compared in pairs; for example, U_i is compared with U_j and the relative importance is evaluated on a scale of 1–9; the implications of the scales are shown in Table 1.

Step 3. Calculate the relative weights of elements following the single criterion and its consistency check.

According to the judgment matrix, the eigenvector corresponding to the maximum eigenvalue of Z is obtained by using linear algebra. The eigenvector obtained is the order of importance of each evaluation factor, and then the normalized factors give the weight distribution. In this paper, the approximate solution technique of the sum-product method is adopted.

(1) Each column is normalized by the judgment matrix, as shown in the following equation:

$$\overline{u}_{ij} = \frac{u_{ij}}{\sum_{K=1}^{M} u_{kj}}, \quad ij = 1, 2, \ldots, m. \quad (2)$$

(2) Each column of the normalized judgment matrix is added by row, as shown in the following equation:

$$\overline{W}_i = \sum_{i=1}^{m} \overline{u}_{ij}, \quad ij = 1, 2, \ldots, m. \quad (3)$$

(3) As shown in equation (4), the vector $\overline{W} = (\overline{W}_1, \overline{W}_2, \ldots \overline{W}_m)^T$ is normalized:

$$a_i = \frac{\overline{W}_i}{\sum_{j=1}^{m} \overline{W}_j}, \quad ij = 1, 2, \ldots, m, \quad (4)$$

$A = (a_1, a_2, a_1)$ obtained in turn is the eigenvector.

(4) As shown in equation (5), the maximum eigenvalue $\lambda_{\max}$ is calculated:

$$\lambda_{\max} = \frac{1}{m} \sum_{i=1}^{m} \frac{(TA)_i}{a_i}. \quad (5)$$

(5) Consistency judgment: to verify whether the judgment matrix results have satisfactory consistency, the value of consistency ratio (CR) is used for judgment, as shown in the following equation:

$$\begin{aligned} \mathrm{CR} &= \frac{\mathrm{CI}}{\mathrm{RI}}, \\ \mathrm{CI} &= \frac{\lambda_{\max} - n}{n - 1}, \end{aligned} \quad (6)$$

where CI is the consistency indicator; *RI* is the random index determined by the number of evaluation factors in the judgment matrix (Table 2); $\lambda_{\max}$ is the maximum eigenvalue of the judgment matrix; and n is the number of indicators. When CR < 0.1, the measures of the consistency levels of the judgment matrix-based results are satisfactory, which signifies that the weight distributions are reasonable and reliable. Otherwise, the matrix must be restructured until the consistency is satisfied.

Step 4. Calculate the element relative weights following the total criterion and its consistency check.

With the hierarchical ranking, the weight of each influencing factor relative to the overall goal is calculated, generally by using the top-down method. Subsequently, the consistency of the final synthesized results is checked to judge the overall consistency.

Table 1: Meaning of 1–9 scales.

Scale	Meaning
1	i has the same importance, or i or j compares to itself
3	i is slightly more important than j
5	i is obviously more important than j
7	i is much more important than j
9	i is extraordinarily more important than j
2, 4, 6, 8	Scales between two consecutive scales given above
Reciprocal	Contrast to the above condition, namely, j is more important than i

Table 2: Values of RI.

N	1	2	3	4	5	6	7	8	9
RI	0	0	0.58	0.94	1.12	1.24	1.32	1.41	1.45

3.2. The Scoring Method. The scoring method is used to calculate the comprehensive evaluation score of water inrush and determine the risk level of water inrush. First, the factors that affect the development of things are decomposed into a number of evaluation indexes (U_1, U_2, . . ., U_n). Second, each evaluation index is divided into several basic evaluation factors (C_1, C_2, . . ., C_n), and the scores of the impact of each basic evaluation index or evaluation factor on the development of things are determined according to the quantitative criteria. Finally, the risk value of the water inrush is obtained with the reverse-order superposition method, which is a linear combination relationship; the final evaluation is performed in combination with the actual analysis. The specific methods of the reverse-order superposition method are given by equations (7) and (8):

$$\mathrm{TRV} = \sum_{n=1}^{\infty} W_{un} * f(U_n), \tag{7}$$

$$f(U_n) = \sum_{n=1}^{\infty} W_{cn} * f(C_n), \tag{8}$$

where the risk value of the water inrush (i.e., TRV) is the comprehensive evaluation index of the water inrush phenomenon; the higher the TRV value, the greater the possibility of water inrush in the tunnel; U_n is the quantitative score of each evaluation index; W_{un} is the weight of each evaluation index; C_n is the quantitative score of the basic evaluation factors; W_{cn} is the weight of each basic evaluation factor.

3.3. Model Analysis. More than 100 cases of water inrush in tunnels in China have been systematically summarized and analyzed mainly based on the variation characteristics and occurrence conditions of water inrush in the tunnel [16, 35–38]. The tunnel water inrush disaster is caused by the effect of tunneling engineering and its interaction with the groundwater environment. Formation lithology is the basis of groundwater storage. The level of the surrounding rock and the lithology of the stratum in which it is located are different. Topography conditions play an important role in groundwater recharge, runoff, and discharge and serve as an important factor affecting the alternation of the groundwater cycle. Geological structure conditions are the dominant factor controlling the direction of groundwater burial, distribution, and movement. Because the location of the tunnel section in the geological structure varies, the stratigraphic production and catchment area in the tunnel sections also significantly vary. The length and burial depth of the tunnel are external factors affecting the formation of the disaster; the longer the tunnel extends in the construction process, the more hydrogeological units and rock layers it traverses; the deeper the tunnel, the larger the catchment area, runoff, and recharge area of the tunnel site. Karst development is an intrinsic factor affecting the water inrush phenomenon.

In this paper, a static water inrush disaster evaluation model of the Micangshan tunnel is established taking into consideration the engineering geological conditions, tunnel section characteristics, and hydrogeological conditions of the tunnel, as well as the statistical analysis of the type of water inrush development. These characteristics are mainly classified as formation lithology (U_1), topography conditions (U_2), geological structure conditions (U_3), tunnel length and buried depth (U_4), and karst development (U_5). These are further divided into five evaluation indicators and 12 evaluation factors (C_1, C_2, C_3, C_4, C_5, C_6, C_7, C_8, C_9, C_{10}, C_{11}, C_{12}). The AHP hierarchical structure model of the water inrush disaster is shown in Figure 7. The level of water inrush disaster is divided into five types, namely, very low risk (risk level I), low risk (risk level II), medium risk (risk level III), high risk (risk level IV), and extremely high risk (risk level V).

Experts' judgment questionnaire is a key point of AHP. There are two approaches to do experts questionnaire: (1) one is the pairwise comparison, proposed by Saaty [34], improved by Li et al. [39]; (2) another method to do questionnaire is to use table comparison proposed by Lyu et al. [40]. The paper used the second method to conduct the questionnaire, which can not only get the appropriate experts' reply but also determine the fuzzy number based on experts' replies. The authors selected six experienced experts with expertise in hydrogeological geological and tunnel engineering to assess the water inrush risk of Micangshan tunnel.

As shown in Tables 3–8, the judgment matrix of the index layer can be calculated. The largest eigenvalue ($\lambda_{\max}$) of the judgment matrix can be calculated by equation (5), and the CR can be calculated and verified by equation (6). The other judgment matrices of the subindex layer to the index

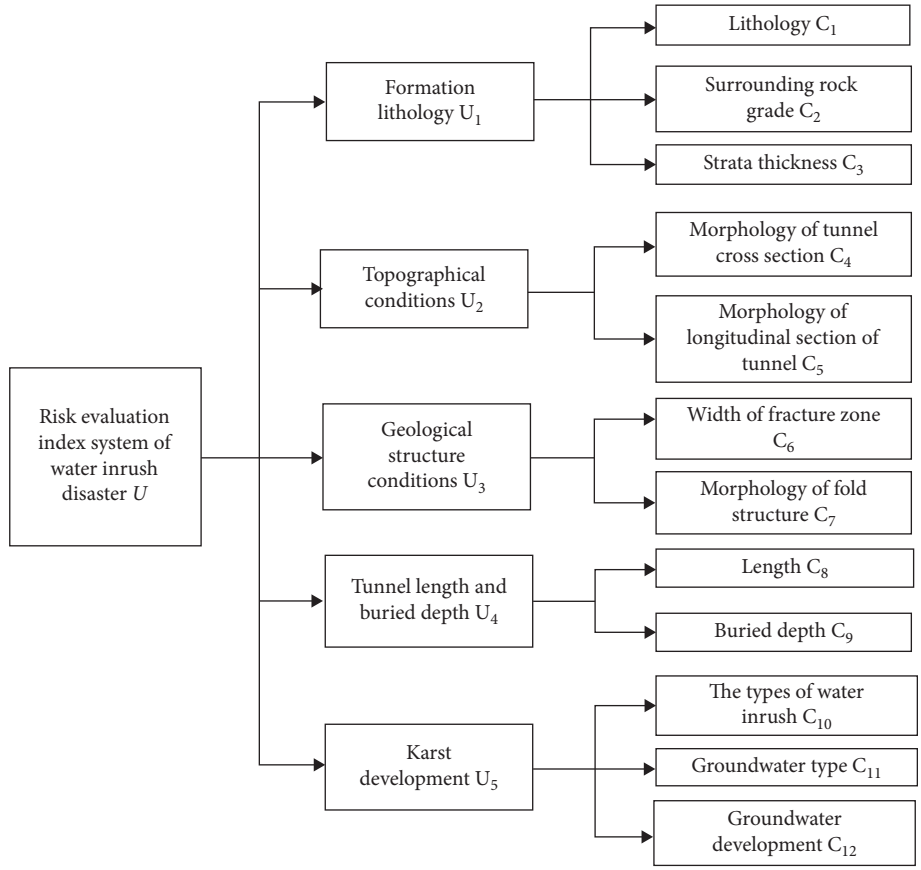

Figure 7: AHP structure model of inrush water intensity.

Table 3: Primary index judgment matrix in U.

	U_1	U_2	U_3	U_4	U_5
U_1	1	7	3	9	5
U_2	1/7	1	1/5	3	1/3
U_3	1/3	5	1	7	5
U_4	1/9	1/3	1/7	1	1/5
U_5	1/5	3	1/5	5	1

layer can also be obtained. In addition, the weight of each judgment matrix can be calculated using the aforementioned method. As shown in Tables 9 and 10, the weight values of the primary and secondary evaluation indexes in this level are calculated separately, and the rationality of the CR is calculated and verified. The CR is less than 0.1, which indicates that the judgment matrix is consistent.

According to the degree and range of disaster causing factors in the evaluation index, the quantitative value of disaster causing factors is determined (see Table 11) [41–43]. At least five tunnel engineering experts are selected for scoring based on the field geological and hydrogeological conditions. The average score of each evaluation index is calculated based on the scores of all the experts, which can improve the accuracy of the final score of each index. Using equations (7) and (8) and the determined weights of the evaluation indexes, the risk value of the water inrush (TRV) is calculated using the scoring method as follows:

$$\begin{aligned} \mathrm{TRV} &= 5 * \left(0.5 * U_1 + 0.06 * U_2 + 0.29 * U_3 + 0.03 * U_4 * 0.12 * U_5\right), \\ &\begin{cases} U_1 = 0.63C_1 + 0.11C_2 + 0.26C_3, \\ U_2 = 0.83C_4 + 0.17C_5, \\ U_3 = 0.25C_6 + 0.75C_7, \\ U_4 = 0.5C_8 + 0.5C_9, \\ U_5 = 0.65C_{10} + 0.07C_{11} + 0.28C_{12}. \end{cases} \end{aligned} \tag{9}$$

The maximum score of U_n is 20. This score must be increased by five times to meet the target TRV value of 100. According to the THR value, the risk grade can be divided into five grades; the higher the score, the higher the level of risk of the disaster, as shown in Table 12.

4. Method of Dynamic Risk Prediction of Water Inrush Phenomenon

The dynamic prediction of the water inrush phenomenon is based on the risk grade of static water inrush, and the advance prediction method is used to determine and analyze the location of the water inrush position in the construction stage. The dynamic prediction of the tunnel water inrush disaster is realized through an integrated advanced prediction method that combines the long distance (e.g., TSP, TRT) and short distance (e.g., GPR, TEM, infrared water detection method, advanced drilling) prediction methods.

Table 4: Secondary index judgment matrix in U_1.

	C_1	C_2	C_3
C_1	1	5	3
C_2	1/5	1	1/3
C_3	1/3	3	1

Table 5: Secondary index judgment matrix in U_2.

	C_4	C_5
C_4	1	5
C_5	1/5	1

Table 6: Secondary index judgment matrix in U_3.

	C_6	C_7
C_6	1	1/3
C_7	3	1

Table 7: Secondary index judgment matrix in U_4.

	C_8	C_9
C_8	1	1
C_9	1	1

Table 8: Secondary index judgment matrix in U_5.

	C_{10}	C_{11}	C_{12}
C_{10}	1	7	3
C_{11}	1/7	1	1/5
C_{12}	1/3	5	1

Table 9: Calculation results of hierarchical single sorting.

Sorting layer			W			λ_{max}	CI	RI	CR
V-U	0.50	0.06	0.29	0.03	0.12	5.3537	0.0884	1.12	0.079
U_1-C	0.63	0.11	0.26			3.0385	0.01925	0.58	0.033
U_2-C	0.83	0.17				2	0	0	0
U_3-C	0.25	0.75				2	0	0	0
U_4-C	0.50	0.5				2	0	0	0
U_5-C	0.65	0.07	0.28			3.065	0.0325	0.58	0.056

Table 10: Hierarchical total sorting weights.

U-C *V-U*	U_1 0.50	U_2 0.06	U_3 0.29	U_4 0.03	U_5 0.12	Total sorting weight
C_1	0.63	0	0	0	0	0.32
C_2	0.11	0	0	0	0	0.05
C_3	0.26	0	0	0	0	0.13
C_4	0	0.83	0	0	0	0.05
C_5	0	0.17	0	0	0	0.01
C_6	0	0	0.25	0	0	0.073
C_7	0	0	0.75	0	0	0.217
C_8	0	0	0	0.50	0	0.015
C_9	0	0	0	0.50	0	0.015
C_{10}	0	0	0	0	0.65	0.078
C_{11}	0	0	0	0	0.07	0.008
C_{12}	0	0	0	0	0.28	0.034

Note. CI = 0.0139, RI = 0.3596, and CR = 0.038.

Table 11: Risk grade system evaluation of the water inrush disaster index.

First-grade evaluation index	Second-grade evaluation index	Quantitative value of disaster causing factors				
U_1	C_1	No fissure hard rock	Mudstone, sandstone, shale	Argillaceous siltstone, sandy mudstone, shale	Dolomite, argillaceous limestone, and other soluble rocks	Dolomitic limestone, dolomite,
	Score	0–4	4–8	8–12	12–16	16–20
	C_2	I, II	III	IV	V	VI
	Score	0–4	4–8	8–12	12–16	16–20
	C_3 (cm)	Thick layer	Middle-thick layer	Middle layer	Thin layer	Unconsolidated layers
	Score	0–8	8–12	12–15	15–18	18–20
U_2	C_4	Convex type	Flat type	Single slope type	Parallel type below the side of the valley	Parallel type below the valley
	Score	0–8	8–12	8–12	15–18	18–20
	C_5	Convex type	Flat type	Mixed type	Depression type	River crossing type
	Score	0–6	6–10	10–14	14–17	17–20
U_3	C_6 (m)	< 1.5	1.5–3	3–5 or contact surfaces of different rock	5–8	> 8
	Score	0–6	6–10	10–14	14–17	17–20
	C_7	Other parts of fold structure	Wing of the gently dipping fold structure	Wing of the steep fold structure	Core of the gently dipping fold structure	Core of the steep fold structure
	Score	0–3	3–6	6–10	10–15	15–20
U_4	C_8 (m)	< 200	200–500	500–1000	1000–1500	> 1500
	Score	0–2	2–6	6–14	14–16	16–20
	C_9 (m)	< 100	100–300	300–500	500–700	> 700
	Score	14–20	10–14	6–10	4–6	0–4
U_5	C_{10}	No water inrush	Water inrush in water-bearing crack	Water inrush in fault fracture zone	Water inrush in karst pipeline	Water inrush in karst cave
	Score	0–4	4–12	12–16	16–18	18–20
	C_{11}	Bedrock fissure water	Clastic rock fissure water	Clastic rock fissure water, bedrock fissure water	Karst fissure water, clastic rock fissure water	Karst fissure water, clastic rock fissure water, bedrock fissure water
	Score	0–6	6–10	10–14	14–17	17–20
	C_{12}	Dry	Humid	Dripping	Rainy	Downpour, local inrush water
	Score	0–2	2–8	8–12	12–16	16–20

Table 12: Risk value assessment of water inrush disaster.

Value of TRV	0–20	20–40	40–50	50–70	>70
Risk level	I (very low risk)	II (low risk)	III (medium risk)	IV (high risk)	V (extremely high risk)

Table 13: Conventional advanced geological forecast methods and characteristics.

Category	Method	Distance (m)	Analysis of the characteristics of groundwater detection	Advantage
Geological analysis method	Geological analysis of tunnel face	—	According to the situation of the tunnel face, the water outlet location and flow rate are recorded	Accurate observation of the location and volume of the effluent
	Advanced drilling	10–20	To judge whether there is a water-bearing body in front of the tunnel face by observing whether the borehole is out of water and determining the amount of water flowing out of it	Accurate observation of the water output and water pressure

Table 13: Continued.

Category	Method	Distance (m)	Analysis of the characteristics of groundwater detection	Advantage
Seismic wave method	Tunnel seismic prediction (TSP)	100–150	In the reflection layer, the shear wave velocity (V_s) tends to decrease, the ratio of longitudinal wave velocity to shear wave velocity (V_s/V_p) increases, or Poisson's ratio suddenly increases	Accurate recognition and location of anomalous geological bodies in front of the tunnel face (such as faults, underground rivers, and caves)
	Tunnel reflection tomography (TRT)	100–150		Properties, size, and 3D holographic imaging of faults, fractured zones, karst caves, underground rivers, and other anomalous geological bodies in front of the tunnel face
Electromagnetic method	Ground penetrating radar (GPR)	15–30	Frequency of electromagnetic wave decreases, resulting in multiple strong reflection interfaces, scattering, and diffraction, resulting in cluttered reflection waveforms	Sensitive to fracture zone, lithology, and water-bearing state changes
	Transient electromagnetic method (TEM)	50–80	The resistivity of surrounding rock is obviously lower than that of surrounding rock	Sensitive to low resistor fracture zones filled with water
Other methods	Infrared water detection method	20–30	The detection instrument shows that the curve has a sudden change	Sensitive to water-bearing rock

Table 14: Dynamic risk prediction method of water inrush in tunnel.

Dynamic prediction method	Primary dynamic prediction	Secondary dynamic prediction	Tertiary dynamic prediction
Risk level	I (extremely low-risk area) II (low-risk area)	III (moderate-risk area)	IV (high-risk area) V (extremely high-risk area)
Dynamic risk prediction methods	Geological analysis of the tunnel face; TSP or TRT detection	Geological analysis of the tunnel face; TSP or TRT detection; GPR or TEM or infrared water detection method	Geological analysis of the tunnel face; TSP or TRT detection; GPR or TEM or infrared water detection method; advanced drilling

The long distance means that the predicted distance from the tunnel face is about 100 m, and the short distance means that the predicted distance from the tunnel face is about 30 m. According to the characteristics of each advance prediction method, the diversity of solutions can be reduced and the reliability of detection results can be improved.

4.1. Advanced Prediction Method of the Tunnel. Conventional prediction methods are geological analysis methods (e.g., palm-top geological analysis, advanced drilling), seismic wave methods (e.g., TSP, TRT), electromagnetic methods (e.g., GPR, TEM), and other methods (e.g., infrared water detection method). Each detection method is based on the difference in some properties of the geological medium (such as elasticity, resistivity, and wave velocity). Owing to the limitations and constraints of factors such as the complexity of geological conditions in the crossing area of long and deep-buried tunnels and the multiple solutions of geophysical methods, each advanced prediction method has its own advantages and limitations (see, for example, Table 13). Using only a single advanced prediction method, it is difficult to accurately detect the geological conditions in front of the tunnel. In particular, under the complex geological and hydrogeological conditions such as those in the Micangshan tunnel, it is more important to determine a scientific, effective, and accurate advance geological prediction method [44, 45].

4.2. Dynamic Prediction Method. According to the static evaluation results of water inrush risk in different sections of Micangshan tunnel, the risk levels of different water inrush disasters are determined. Then, the dynamic water inrush disaster prediction method is adopted, with different advanced prediction methods for different risk levels of water inrush disasters to predict the position of water inrush disasters in the construction process. Therefore, three dynamic water inrush prediction methods are divided, namely, primary dynamic prediction, secondary dynamic prediction, and terminal dynamic prediction (Table 14). Based on this, a comprehensive advanced geological prediction system suitable for tunnel engineering is constructed, and the process of dynamic prediction is formed.

5. Model Verification

The buried depth of the K41 + 440–K43 + 080 mileage section of the Micangshan tunnel is 751 m, the lithology mainly comprises dolomite, and the rock is formed in the middle

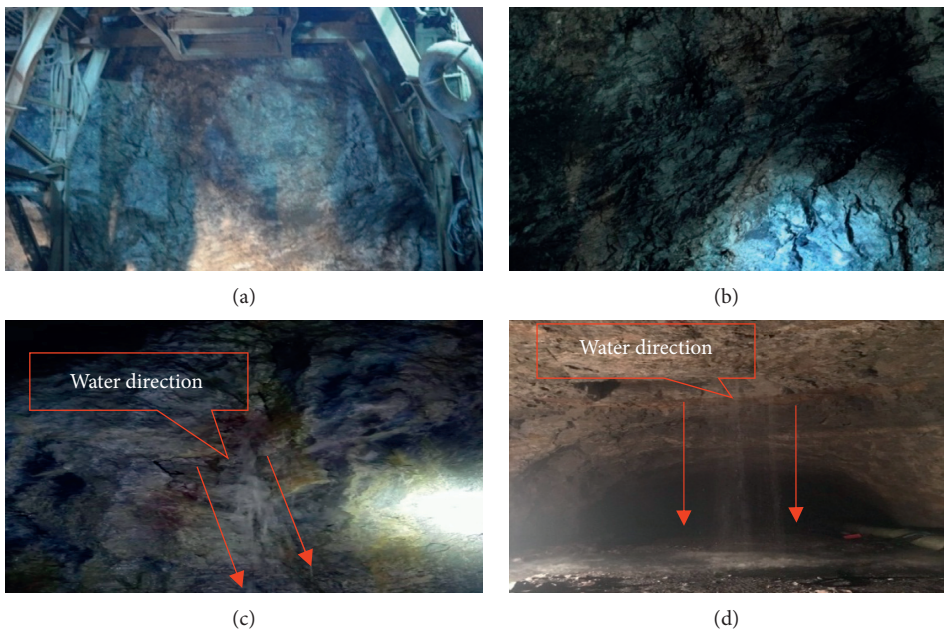

Figure 8: Geological analysis of the tunnel face. (a) Overall drawing of the tunnel face. (b) Right side of the tunnel face. (c) Water gushing from cracks on the left side of the tunnel face. (d) Water pouring downward from the crown.

layer. The sectional view indicates that it is a parallel type below the valley, and the groundwater is karst fissure water, with local water inrush, occurring in water-bearing cracks. The face of the tunnel excavated in the K42 + 480 section is shown in Figure 8. The surrounding rock is mainly dolomite, and the bedding plane is slightly bent and partially broken because of tectonic movement. The joints in the tunnel face are nonuniformly distributed, the source of the vault is rain, and water gushes from the cracks on the left side of the face of the tunnel. According to the specifications for design of highway tunnels, the surrounding rock is of level V. The quantitative and qualitative analysis of the static evaluation model provides a TRV value of 75, implying that this tunnel area has grade-V risk. As shown in Table 14, tertiary dynamic prediction is adopted in the area, including geological analysis of the tunnel face analysis, TSP detection, the GPR water detection method, and advanced drilling.

In the TSP method, seismic waves are generated by an artificially excited source and propagated in front of the tunnel along the tunnel axis. When unfavorable geological bodies (such as karst caves or fissures) are encountered in front of the tunnel face, the waves are reflected, which are received by highly sensitive sensors. According to the reflection time, propagation speed, and waveform of the reflected waves, different data characteristics are processed by TSPwin Light software to predict the location of the unfavorable geological bodies. As shown in Figure 9(a), the physical and mechanical parameter results obtained by TSP for the K42 + 510–K42 + 540 section clearly show that the velocities of both P and S waves decrease and the waveforms are abnormal. The ratio of P to S waves increases, while the elastic modulus and density decrease. The reflection layer produced by TSP in the corresponding section indicates the significant enhancement of the negative reflection region (Figure 9(b)). The prediction results obtained by TSP for the K42 + 510–K42 + 540 section clearly indicate that there is considerable fracture development and a large amount of water content in this section.

In the GPR method, the distribution law of rock mass media is determined by transmitting pulsed electromagnetic waves in a certain frequency range. Through the comprehensive analysis and processing of radar data and complex meteorological elements, various characteristic parameters of disaster sources can be obtained, and adverse geological structures such as caves and faults in tunnels can be detected. According to the key water inrush areas predicted by the TSP method, SIR3000 GPR is used to detect geological structures in the K42 + 510–K42 + 540 section. Two measuring lines are used for measurement to ensure high detection accuracy. The radar is moved from left to right in uniform motion during implementation while avoiding the phenomena of disengaging, stagnation, and sudden drive as much as possible. The velocity and position of the two lines are consistent. The GPR interpretation results for the K42 + 510–K42 + 540 section show that the radar-reflected wave amplitude increases significantly and the strong reflection interface is clear (see Figure 10). This indicates broken rock mass in the cave section, likely containing voids and cavernous geological structures. The K42 + 492 section is mainly composed of medium dolomite, and advanced drilling is used in this section. The advanced drilling results indicate that the drilling speed increases to a large value and remains constant. Water gushes out from the pipe core, with a jet distance of approximately 1 m (Figure 11). This area has well-developed joints and fissures and high water pressure, and the groundwater gushes out through boreholes.

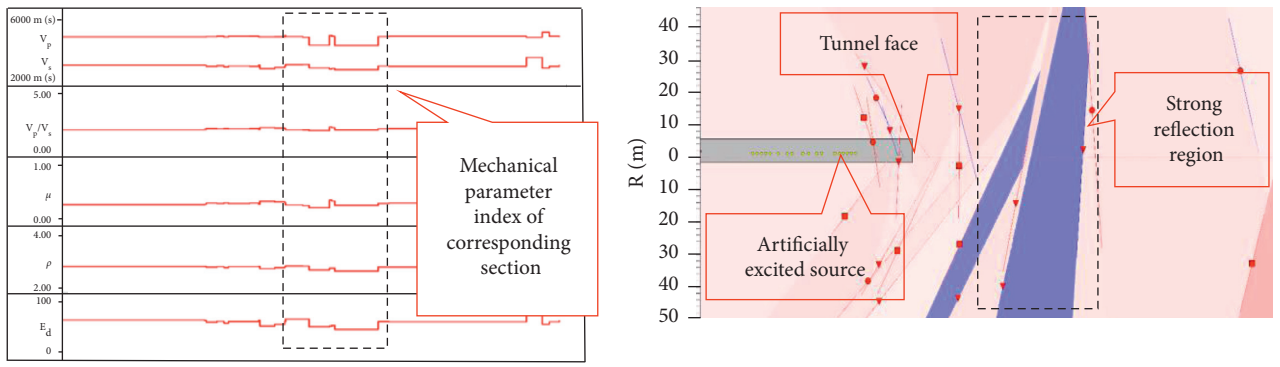

Figure 9: TSP advanced prediction interpretation. (a) TSP physical and mechanical parameters result map. (b) TSP reflective layer map.

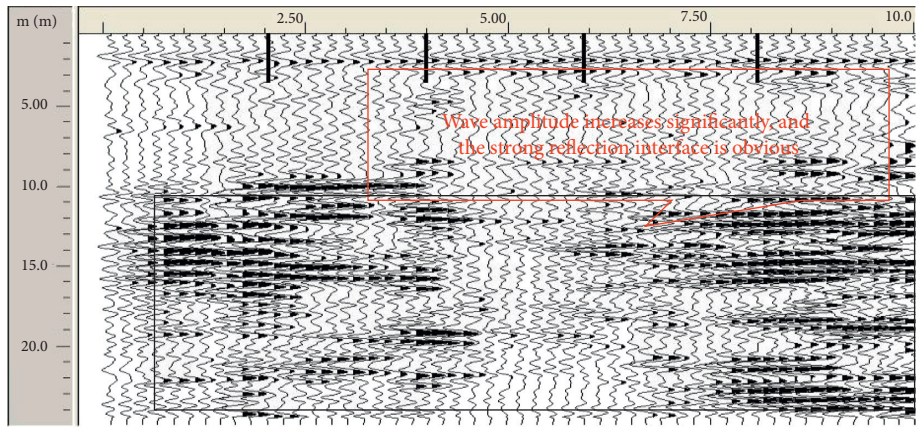

Figure 10: Ground penetrating radar interpretation map of the K42 + 510–K42 + 540 section.

Figure 11: Water gushing during advanced drilling.

When the tunnel is excavated to the K42 + 530 mileage section, the tunnel face mainly comprises dolomite, which is relatively weak and the cracks are developed as a whole. According to the static evaluation results of water inrush and the interpretation of the dynamic evaluation results, high risk of water inrush is considered highly likely to occur in this section. The surrounding rock is easy to deform after excavation and unloading, and the unloading fissure gradually expands to form a seepage or outburst channel for groundwater discharge. As shown in Figure 12, a large amount of water gushes out of the boreholes and cracks, and water inrush continuously increases at approximately 800 m^3/h on average. As a result, the tunnel is flooded 60 m behind the work face. During advanced drilling, to release high-pressure water stored in the surrounding rock beforehand, emergency evacuation of workers and equipment was carried out and timely drainage measures were undertaken in the tunnel, avoiding any catastrophic water gushing accident. The static-dynamic water inrush risk assessment method realizes the accurate prediction of water inrush risk in karst tunnels. It

Figure 12: Photos of water gushing from actual excavation to K42 + 530.

would considerably reduce the possibility of water inrush and provide the design basis for the treatment.

6. Conclusions

(1) Based on the geological and hydrogeological conditions of the Micangshan tunnel, four types of water inrush were identified: water inrush in water-bearing cracks, fault fracture zones, karst pipelines, and karst caves.

(2) By considering the qualitative and quantitative factors, 5 first-level evaluation indexes and 12 second-level evaluation indexes were extracted, which form the tunnel water inrush risk assessment indexes. Based on these indexes, a static water inrush disaster risk assessment model was established. The risk of the water inrush disaster in terms of the TRV values was graded as I (very low risk), II (low risk), III (medium risk), IV (high risk), and V (extremely high risk). To accurately identify occurrence characteristics and the damage level of the water-bearing body, the sensitivity of the advanced prediction method to groundwater was summarized and analyzed, and the following three dynamic prediction methods were established: primary dynamic prediction, secondary dynamic prediction, and terminal dynamic prediction methods.

(3) The excavation of the K42 + 510–K42 + 540 mileage section of the Micangshan tunnel was assessed using the static water inrush risk assessment method and was judged as high risk. Based on the dynamic evaluation model and using the terminal dynamic prediction method in the construction process, it can be inferred that rich fissure water develops before the tunnel face, and the connectivity between the tunnel face and groundwater is good. The accuracy of the static-dynamic water inrush disaster risk assessment and prediction method was verified and the rationality and applicability of the method were proved.

Data Availability

The underlying data supporting the results of our study are unavailable.

Conflicts of Interest

The authors declare that they have no conflicts of interest.

Acknowledgments

This research was financially supported by the National Natural Science Foundation of China (nos. 41807255, 41772329, and U19A20111), the research fund of the State Key Laboratory of Geohazard Prevention and Geoenvironment Protection Independent Research Project (SKLGP2020Z010), and Sichuan Science and Technology Project (no. 2019YJ0465).

References

[1] K. Suzuki, E. Nakata, M. Minami et al., "Estimation of the zone of excavation disturbance around tunnels, using resistivity and acoustic tomography," *Exploration Geophysics*, vol. 35, no. 1, pp. 62–69, 2004.

[2] M. Taromi, A. Eftekhari, J. K. Hamidi, and A. Aalianvari, "A discrepancy between observed and predicted NATM tunnel behaviors and updating: a case study of the Sabzkuh tunnel," *Bulletin of Engineering Geology and the Environment*, vol. 76, no. 2, pp. 713–729, 2016.

[3] A. Kaya, K. Karaman, and F. Bulut, "Geotechnical investigations and remediation design for failure of tunnel portal section: a case study in northern Turkey," *Journal of Mountain Science*, vol. 14, no. 6, pp. 1140–1160, 2017.

[4] D.-X. Liang, Z.-Q. Jiang, S.-Y. Zhu, Q. Sun, and Z.-W. Qian, "Experimental research on water inrush in tunnel construction," *Natural Hazards*, vol. 81, no. 1, pp. 467–480, 2016.

[5] D. Huang, Z. Liu, and W. Wang, "Evaluating the impaction of coal mining on ordovician karst water through statistical methods," *Water*, vol. 10, no. 10, pp. 1409–1425, 2018.

[6] D. Mao, Z. Liu, W. Wang et al., "An application of hydraulic tomography to a deep coal mine: combining traditional pumping tests with water inrush incidents," *Journal of Hydrology*, vol. 567, pp. 1–11, 2018.

[7] Y.-H. Chen, S. Cheng, L.-P. Li, J.-y. Yang, H.-l. Liu, and W.-f. Tu, "Applicability analysis of microseismic technology in tunnel water inrush monitoring," *KSCE Journal of Civil Engineering*, vol. 25, no. 7, pp. 2737–2747, 2021.

[8] N. Dastanboo, X.-Q. Li, and H. Gharibdoost, "Investigation on the accuracy of ground penetrating radar in the tunnel based on improved analectic hierarchy process," *International Nano Letters*, vol. 11, no. 1, pp. 69–83, 2021.

[9] H.-M. Lyu, W.-J. Sun, S.-L. Shen, and A. Arulrajah, "Flood risk assessment in metro systems of mega-cities using a gis-based modeling approach," *The Science of the Total Environment*, vol. 626, pp. 1012–1025, 2018.

[10] H.-M. Lyu, S.-L. Shen, A.-N. Zhou, and W.-H. Zhou, "Flood risk assessment of metro systems in a subsiding environment using the interval FAHP-FCA approach," *Sustainable Cities and Society*, vol. 50, Article ID 101682, 2019.

[11] H.-M. Lyu, W.-H. Zhou, S.-L. Shen, and A.-N. Zhou, "Inundation risk assessment of metro system using AHP and TFN-AHP in Shenzhen," *Sustainable Cities and Society*, vol. 56, Article ID 102103, 2020.

[12] H.-M. Lyu, S.-L. Shen, A. Zhou, and J. Yang, "Risk assessment of mega-city infrastructures related to land subsidence using improved trapezoidal FAHP," *The Science of the Total Environment*, vol. 717, Article ID 135310, 2020.

[13] A.-T. Li and J.-W. Lin, "Constructing core competency indicators for clinical teachers in Taiwan: a qualitative analysis and an analytic hierarchy process," *BMC Medical Education*, vol. 14, no. 1, p. 75, 2014.

[14] Y. Wang, W. Yang, M. Li, and X. Liu, "Risk assessment of floor water inrush in coal mines based on secondary fuzzy comprehensive evaluation," *International Journal of Rock Mechanics and Mining Sciences*, vol. 52, no. 6, pp. 50–55, 2012.

[15] Y. Xue, Z. Li, S. Li et al., "Water inrush risk assessment for an undersea tunnel crossing a fault: an analytical model," *Marine Georesources & Geotechnology*, vol. 37, no. 7, pp. 816–827, 2018.

[16] K. Zhang, W. Zheng, C. Xu, and S. Chen, "An improved extension system for assessing risk of water inrush in tunnels in carbonate karst terrain," *KSCE Journal of Civil Engineering*, vol. 23, no. 5, pp. 2049–2064, 2019.

[17] H. Wu, D. Ma, A. J. S. Spearing, and G.-Y. Zhao, "Fracture response and mechanisms of brittle rock with different numbers of openings under uniaxial loading," *Geomechanics and Engineering*, vol. 25, no. 6, pp. 481–493, 2021.

[18] D. Ma, J.-J. Wang, X. Cai et al. "Effects of height/diameter ratio on failure and damage properties of granite under coupled bending and splitting deformation," *Engineering Fracture Mechanics*, vol. 220, Article ID 106640, 2019.

[19] Q. Li and W. Sui, "Risk evaluation of mine-water inrush based on principal component logistic regression analysis and an improved analytic hierarchy process," *Hydrogeology Journal*, vol. 29, no. 3, pp. 1299–1311, 2021.

[20] M. A. M. Ismail, T. A. Majid, C. O. Goh, S. P. Lim, and C. G. Tan, "Geological assessment for tunnel excavation under river with shallow overburden using surface site investigation data and electrical resistivity tomography," *Measurement*, vol. 144, pp. 260–274, 2019.

[21] K.-I. Song, G.-C. Cho, and S.-B. Chang, "Identification, remediation, and analysis of karst sinkholes in the longest railroad tunnel in South Korea," *Engineering Geology*, vol. 135-136, pp. 92–105, 2012.

[22] S. C. Li, Z. Q. Zhou, Z. H. Ye, L. P. Li, Q. Q. Zhang, and Z. H. Xu, "Comprehensive geophysical prediction and treatment measures of karst caves in deep buried tunnel," *Journal of Applied Geophysics*, vol. 116, pp. 247–257, 2015.

[23] A. Alimoradi, A. Moradzadeh, R. Naderi, M. Z. Salehi, and A. Etemadi, "Prediction of geological hazardous zones in front of a tunnel face using TSP-203 and artificial neural networks," *Tunnelling and Underground Space Technology*, vol. 23, no. 6, pp. 711–717, 2008.

[24] T. Yamatoto, S. Shirasagi, Y. Yokota, and Y. Koizumi, "Imaging geological conditions ahead of a tunnel face using three-dimensional seismic reflector tracing system," *International Journal of the JCRM*, vol. 6, no. 1, pp. 23–31, 2011.

[25] R. Ahmadi, N. Fathianpour, and G.-H. Norouzi, "Detecting physical and geometrical parameters of some common geotechnical targets through their effects on GPR responses," *Arabian Journal of Geosciences*, vol. 8, no. 7, pp. 4843–4854, 2015.

[26] S.-H. Baek, S.-S. Kim, J.-S. Kwon, and E. S. Um, "Ground penetrating radar for fracture mapping in underground hazardous waste disposal sites: a case study from an underground research tunnel, South Korea," *Journal of Applied Geophysics*, vol. 141, pp. 24–33, 2017.

[27] M.-M. Liu, Z.-H. Liu, D. Zhou, R.-Y. Lan, and H. Wu, "Recognition method of typical anomalies during karst tunnel construction using GPR attributes and Gaussian processes," *Arabian Journal of Geosciences*, vol. 13, no. 16, pp. 4843–4854, 2020.

[28] R. M. Corbeanu, G. A. McMechan, R. B. Szerbiak, and K. Soegaard, "Prediction of 3-D fluid permeability and mudstone distributions from ground-penetrating radar (GPR) attributes: example from the Cretaceous Ferron Sandstone Member, east-central Utah," *Geophysics*, vol. 67, no. 5, pp. 1495–1504, 2002.

[29] L. Liu, Z.-M. Shi, M. Peng et al., "A borehole multifrequency acoustic wave system for karst detection near piles," *Journal of Applied Geophysics*, Article ID 104051, 2020.

[30] S. Li, B. Liu, X. Xu et al., "An overview of ahead geological prospecting in tunneling," *Tunnelling and Underground Space Technology*, vol. 63, pp. 69–94, 2017.

[31] E. Forte, M. Pipan, D. Casabianca, R. Di Cuia, and A. Riva, "Imaging and characterization of a carbonate hydrocarbon reservoir analogue using GPR attributes," *Journal of Applied Geophysics*, vol. 81, pp. 76–87, 2012.

[32] S.-C. Li, K. Wang, L.-P. Li, Z. Q. Zhou, S. Shi, and S. Liu, "Mechanical mechanism and development trend of water-inrush disasters in karst tunnels," *Chinese Journal of Theoretical and Applied Mechanics*, vol. 49, no. 1, pp. 22–30, 2017, in Chinese.

[33] Y.-G. Xue, F.-M. Kong, S.-C. Li et al., "Water and mud inrush hazard in underground engineering: genesis, evolution and prevention," *Tunnelling and Underground Space Technology*, vol. 114, Article ID 103987, 2021.

[34] T. L. Saaty, "A scaling method for priorities in hierarchical structures," *Journal of Mathematical Psychology*, vol. 15, no. 3, pp. 234–281, 1977.

[35] S.-C. Li, Z.-Q. Zhou, L.-P. Li, Z.-h. Xu, Q.-q. Zhang, and S.-s. Shi, "Risk assessment of water inrush in karst tunnels based on attribute synthetic evaluation system," *Tunnelling and Underground Space Technology*, vol. 38, pp. 50–58, 2013.

[36] S. C. Li, J. Wu, Z. H. Xu, L. Zhou, and B. Zhang, "A possible prediction method to determine the top concealed karst cave based on displacement monitoring during tunnel construction," *Bulletin of Engineering Geology and the Environment*, vol. 78, no. 1, pp. 341–355, 2019.

[37] X. Huang, S.-C. Li, Z.-H. Xu, M. Guo, and Y.-C. Chen, "Assessment of a concealed karst cave's influence on karst tunnel stability: a case study of the huaguoshan tunnel, China," *Sustainability*, vol. 10, no. 7, p. 2132, 2018.

[38] S. Wang, S. Li, L. Li et al., "Study on early warning method for water inrush in tunnel based on fine risk evaluation and hierarchical advance forecast," *Geosciences*, vol. 9, no. 9, pp. 392–412, 2019.

[39] F. Li, K. K. Phoon, X. Du, M. Zhang, and M.-J. Zhang, "Improved AHP method and its application in risk

identification," *Journal of Construction Engineering and Management*, vol. 139, no. 3, pp. 312–320, 2013.

[40] H.-M. Lyu, S. M. Asce, W.-J. Sun, A. M. Asce, S.-L. Shen, and A.-N. Zhou, "Risk assessment using a new consulting process in fuzzy AHP," *Journal of Construction Engineering and Management, ASCE*, vol. 146, no. 3, Article ID 04019112, 2020.

[41] Y.-C. Wang, X. Yin, H.-W. Jing, R. Liu, and H. Su, "A novel cloud model for risk analysis of water inrush in karst tunnels," *Environmental Earth Sciences*, vol. 75, Article ID 103987, 2016.

[42] T. Song, *Study on Prediction and Treatment Measures of Water Inrush in Micangshan Tunnel*, Chengdu University of Technology, Chengdu, China, 2015, in Chinese.

[43] Y.-X. Peng, L. Wu, Q.-J. Zuo, C.-H. Chen, and Y. Hao, "Risk assessment of water inrush in tunnel through water-rich fault based on AHP-Cloud model," *Geomatics, Natural Hazards and Risk*, vol. 11, no. 1, pp. 301–317, 2017.

[44] L.-C. Nie, Y.-H. Zhang, M.-X. Su et al., "Comprehensive ahead prospecting of tunnels in severely weathered rock mass environments with high water inrush risk: a case study in Shaanxi Province," *Advances in Civil Engineering*, vol. 2020, Article ID 8867382, 10 pages, 2020.

[45] L. Bu, S. Li, S. Shi et al., "Application of the comprehensive forecast system for water-bearing structures in a karst tunnel: a case study," *Bulletin of Engineering Geology and the Environment*, vol. 78, no. 1, pp. 357–373, 2019.